Bio-Spectroscopic Imaging Provides Evidence of Hippocampal Zn Deficiency and Decreased Lipid Unsaturation in an Accelerated Ageing Mouse Model

Fimognari, N,[1,2α] Hollings, A.,[1,3,α] Lam, V.,[1,4] Tidy, R.J.,[1,3] Kewish, C.M.,[5] Albrecht, M.A.,[1] Takechi, R,[1,4] Mamo, J.C.,[1,4] Hackett, M.J.[*1,3]

[1] Curtin Health Innovation Research Institute, Curtin University, Bentley, WA 6102, AUS

[2] School of Biomedical Sciences, Curtin University, Bentley, WA 6102, AUS

[3] Curtin Institute for Functional Molecules and Interfaces, School of Molecular and Life Science, Curtin University, Bentley, WA 6845, AUS

[4] School of Public Health, Curtin University, Bentley, WA 6102, AUS

[5] Australian Nuclear Science and Technology Organisation, 800 Blackburn Road, Clayton, VIC, AUS 3168

[α]Fimognari and Hollings contributed equally to this work and are co-1st-authors, listed in alphabetical order.

***** Corresponding Author: E-mail: mark.j.hackett@curtin.edu.au Tel.: +61 8 9266 3102

KEYWORDS: FTIR, XFM, Dementia, Ageing, Metals, Metabolism

ABSTRACT

Western society is facing a health epidemic due to the increasing incidence of dementia in ageing populations, and there are still few effective diagnostic methods, minimal treatment options, and no cure. Ageing is the greatest risk factor for memory loss that occurs during the natural ageing process, as well as being the greatest risk factor for neurodegenerative disease such as Alzheimer's disease. Greater understanding of the biochemical pathways that drive a healthy ageing brain towards dementia (pathological ageing or Alzheimer's disease), is required to accelerate the development of improved diagnostics and therapies. Unfortunately, many animal models of dementia model chronic amyloid precursor protein over-expression, which although highly relevant to mechanisms of amyloidosis and familial Alzheimer's disease, does not model well dementia during the natural ageing process. A promising animal model reported to model mechanisms of accelerated natural ageing and memory impairments, is the senescence accelerated murine prone strain 8 (SAMP8), which has been adopted by many research group to study the biochemical transitions that occur during brain ageing. A limitation to traditional methods of biochemical characterisation is that many important biochemical and elemental markers (lipid saturation, lactate, transition metals) cannot be imaged at meso- or micro-spatial resolution. Therefore, in this investigation we report the first multi-modal biospectroscopic characterisation of the SAMP8 model, and have identified important biochemical and elemental alterations, and co-localisations, between 4 month old SAMP8 mice and the relevant control (SAMR1) mice. Specifically, we demonstrate direct evidence of Zn deficiency within specific sub-regions of the hippocampal CA3 sector, which co-localise with decreased lipid unsaturation. Our findings also revealed colocalisation of decreased lipid unsaturation and increased lactate in the corpus callosum white matter, adjacent to the hippocampus. Such findings may have important implication for future research aimed at elucidating specific biochemical pathways for therapeutic intervention.

INTRODUCTION

Western society is facing a health epidemic due to the increasing incidence of dementia in ageing populations. In 2015, dementia was the cause of a global USD $818 billion health care cost, which is expected to reach USD $2 trillion in 2030.[1] At present there is no cure for dementia, and the greatest risk factor for dementia is age. Therefore, increased understanding of the biochemical and elemental alterations that drive the "switch" from healthy brain ageing towards degenerative pathways and onset of dementia, may help identify therapeutic strategies to minimise or delay dementia in the elderly.

The senescence accelerated murine prone (SAMP) mouse strain is a novel model to study the process of ageing, and factors that drive a "switch" from healthy ageing to dementia.[2-6] The mouse model was a spontaneous occurrence, in a AKR/J mouse line.[5, 6] Following the initial observation of litter mates displaying accelerated ageing, selective breeding was used to develop the SAMP8 and several other SAMP strains. In addition, selective breeding maintained a strain from the initial litter mates that do not show accelerated ageing to the same extent, the senescence accelerated murine resistant strain 1 (SAMR1).[5, 6] Due to multiple genetic differences that occur in both SAMP8 and SAMR1 mice relative to the original AKR/J line, a SAMP8 / SAMR1 comparison is frequently used to identify biochemical and physiological mechanisms specific to the process of accelerated ageing.[5, 6] One of the major advantages of the SAMP model lies in the ability to study biochemical alterations that occur in the ageing brain on a drastically shortened time frame, typically 4 - 12 months, compared to other models, 12 - 24 months in wildtype mice, longer in rats or other rodents.[2, 3, 5-8] A second favourable attribute, specific to the SAMP8 strain (but not all SAMP strains) is that the memory deficits and cognitive decline during ageing occur in the absence of gross overproduction of amyloid precursor protein (APP) and amyloid-β (Aβ) pathology.[6, 9, 10] In other models, substantial research has been conducted into the mechanisms of memory loss arising from Aβ pathology and Aβ-plaque formation, using transgenic models that overproduce APP or Aβ by more than an order of magnitude above wildtype animals.[11-16] Such Aβ overproduction models well familial Alzheimer's disease, and is undoubtedly useful to study Aβ-plaque pathology.[17] However, the transgenic models do not reflect the vast majority of clinical dementia cases, which occur in the elderly humans, without excessively elevated, lifelong cerebral APP or Aβ production.[1] Modest increases in APP or Aβ production have been identified in the ageing human brain,[18] which match well with the modest increase in APP production reported in ageing SAMP8 and wildtype mice.[9, 10, 19-21]

Numerous studies have characterised alterations to brain physiology and biochemistry that occur in the SAMP model. Many of the alterations that occur in SAMP strain reflect well the alterations that occur in other rodent models and in humans. Such alterations include: increased permeability of the blood-brain-barrier (BBB),[7, 8, 22] disturbed lipid homeostasis,[23] accumulation of proteinaceous aggregates;[23] altered energy metabolism favouring lactate production.[24, 25] Typically, these alterations are most prominent within the hippocampus, a brain structure critical for learning and memory. In addition to the above biochemical alterations, there is substantive evidence that accumulation of redox active metals occur during ageing,[26-30] although this has been studied little in the SAMP8 model. Metal accumulation could be harmful during ageing as it catalyses free radical production through Fenton chemistry, driving oxidative stress, lipid oxidation and protein oxidation/aggregation.[26-30] Consequently, there is great interest in further understanding the relationship between brain metal homeostasis and macromolecular homeostasis during ageing, and how it may drive a switch from healthy brain ageing towards memory loss and dementia.

Although the bulk biochemical alterations that occur in the SAMP8 model have been well characterised, much remains unknown about biochemical and elemental alterations that occur at the micro- or meso-scale within distinct sub-regions of the hippocampus. The ability to directly study a wealth of biochemical and elemental parameters at micro- or meso-spatial resolution, without the need

of chemical stains, was a long unfilled niche in the field of neuroscience. However, the modern neuroscientist has access to a suite of bio-spectroscopic imaging techniques that fill this niche, such as X-ray fluorescence microscopy (XFM) and Fourier transform infrared spectroscopy (FTIR). The techniques provide direct *in situ* imaging within *ex vivo* tissue sections, without the need for chemical fixation or staining, which minimises redistribution artefacts due to chemical alterations that can occur with non-direct measurement.[31-36] Further, XFM and FTIR provide the ability to study chemical species that are difficult to image with more traditional methods. XFM elemental mapping has been integrated into numerous studies to determine ion (Cl^-, K^+, and Ca^{2+})[37, 38] and metal (Fe, Cu, Zn)[38-41] within the brain, while FTIR has been used to study cerebral lipid homeostasis,[42-45] protein aggregation (including plaque formation) and metabolic alterations, such as lactate production.[31, 39, 46] The ability to study these biochemical markers has been used to study the pathology of epilespy,[47-50] stroke,[38, 46, 51, 52] Alzheimer's disease,[41-44, 53-59] Parkinson's disease,[60] schizophrenia,[37] multiple sclerosis,[45, 61] prion disease[62-64] and cerebral malaria.[39]

In our ongoing studies we seek to increase understanding of the biochemical and elemental alterations that occur during brain ageing, to help identify potential mechanistic pathways responsible for a switch from healthy ageing towards neurodegeneration and dementia. To do so, we have integrated traditional histology with XFM analysis of ions (Cl^-, K^+, Ca^{2+}) and metals (Fe, Cu, Zn), and FTIR analysis of metabolites (lactate), lipids and protein aggregates. Herein we report our initial observational/phenomenological study, which was designed to characterise elemental and biochemical alterations within the brains of 4 month old adult SAMP8 and SAMR1 mice. We have chosen this age group as it reflects the earliest time point at which mild age-related cognitive decline in this model has been reported, preceding more substantial pathological decline later in life.[3, 65] Due to the importance of the hippocampus for memory function, and the established involvement of the hippocampus in memory loss during dementia, we have focussed our studies to the hippocampus and surrounding white matter (corpus callosum). More specifically, alterations in lipid homeostasis and brain metabolism have been previously reported in SAMP8 mice, however, the exact anatomical location remained unknown. In this study, we have used direct bio-spectroscopic imaging (FTIR) to confirm that biochemical markers of altered metabolism and lipid homeostasis are present in SAMP8 mice, and further, we identify the anatomical locations(s) in which the alterations are most pronounced. Lastly, we have used XFM elemental mapping to test if altered metal levels co-localize with the observed biochemical alterations.

RESULTS & DISCUSSION

Study Design

This study used a multi-modal spectroscopic approach (FTIR and XFM) to image multiple biochemical and elemental parameters within specific anatomical sub-regions of the hippocampus and surrounding corpus callosum white matter, in SAMP8 and SAMR1 mice. Analysis has been conducted on flash-frozen non-fixed brain tissue to preserve the chemical composition as close as possible to the *in vivo* state. FTIR spectroscopic imaging was incorporated into the analytical methodology to reveal biochemical distribution of lactate, and markers of lipid homeostasis, and XFM was incorporated to reveal elemental distribution. (P, S, Cl, K, Ca, Fe, Cu, Zn).

Statistical Analysis

Data in this study was parametric quantitative (XFM) and semi-quantitative (FTIR), derived from discrete anatomical locations within, and surrounding, the hippocampus, for two animal models (SAMP8 and SAMR1 strains, $n = 8$ replicates in each group). Therefore, data were analysed using a 2-Way repeated measures ANOVA (animal strain [between-subjects factor] and anatomic region [within-subjects factor]). A summary of the outcomes from the 2-Way ANOVA are presented in Table 1. Post-hoc comparisons were undertaken in cases where a main-effect only (unsaturated lipids), an interaction effect (Cu and Ca) or an interaction and main effect (Zn and lactate) were found. The *p*-values for statistically significant post-hoc tests are reported in Figures 3 and 5. Corrections for multiple comparisons between anatomic regions was undertaken (described in methods). Post-hoc testing revealed that specific sub-regions of the hippocampus have different contents of Zn, lactate and unsaturated lipids, however, Ca and Cu, which displayed interaction effects only, were not found to be different between SAMP8 and SAMR1 mice within any anatomical sub-region.

Table 1: Two-Way ANOVA Results for the Effect of Animal Strain and Hippocampal Sub-Region on Elemental and Biochemical Content

Dependent Variable	Main Effect (SAMP8 vs SAMR1)	Main Effect (hippocampal sub-region)	Interaction Effect
P	0.0593	<0.0001	0.8403
S	0.1391	<0.0001	0.8920
Cl	0.0685	<0.0001	0.6280
K	0.0622	0.0001	0.8415
Ca	0.1144	<0.0001	0.0164
Fe	0.0892	<0.0001	0.1034
Cu	0.6126	<0.0001	<0.0001
Zn	0.0064	<0.0001	<0.0001
Lipid Ester	0.4074	<0.0001	0.7497
Lipid Methylene	0.3273	<0.0001	0.7969
Unsaturated Lipid	0.0007	<0.0001	<0.0001
Lactate	0.0334	<0.0001	0.3280

"Label Free" Biospectroscopic Imaging Provides Direct Analysis of Hippocampal Biochemical and Elemental Homeostasis

There is a wide breadth of published literature describing bulk biochemical alterations that occur during ageing, including the SAMP model. However, direct characterisation of the anatomical location of the biochemical and elemental alterations is lacking. Our research team is collectively characterising the location of biochemical and elemental alterations that occur across the full time course of SAMP8 and SAMR1 models, as well as wildtype strains, in addition to investigation of the effect lifestyle factors such as diet and exercise have on brain metabolism and metal homeostasis. In this investigation, we report our initial findings at a single time point (4 month old adult

SAMP8/SAMR1 mice), reveal the anatomical location of alterations in metabolic and lipid homeostasis that were previously only characterised on a bulk scale. To quantify biochemical and elemental content of specific anatomical structures, regions of interest were defined based on classical, well defined hippocampal anatomy. The anatomical demarcation of hippocampal sub-regions are presented alongside routine haematoxylin and eosin histology in Figure 1A,B. In this study, XFM data was collected at the micron scale (~3 µm spatial resolution), which allowed the average elemental content to be determined for 20 specific hippocampal sub-regions, including the corpus callosum white matter that surrounds the hippocampus proper (Figure 1C). FTIR spectroscopic imaging data was collected at the meso-scale (25 µm spatial resolution), and therefore, biochemical alterations were quantified on a less resolved spatial scale, for 7 hippocampal sub-regions, including the corpus callosum white matter that surrounds the hippocampus proper (Figure 1D). The anatomical sub-regions and their abbreviations are defined in the caption of Figure 1.

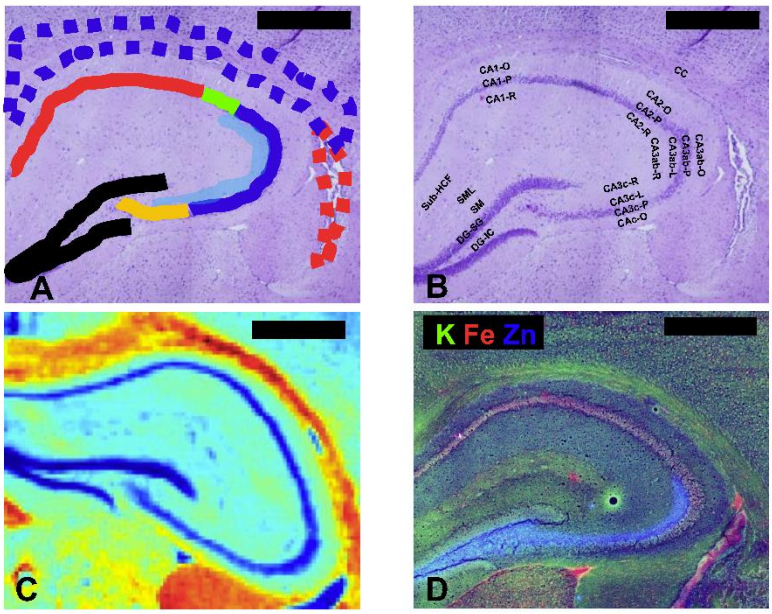

Figure 1: Neuro-anatomy of the hippocampus is observed in routine histology, as well as XFM and FTIR imaging. (A) Regions of interest for which average FTIR spectra were calculated: CA1 subsector (red); CA2 (green); CA3 (dark blue); Hilus/CA4 (Yellow); DG (black); CA3 Mossy Fibers (light blue); Corpus Calossum white matter (blue dashes); lateral ventricle (red dashes). Due to heterogenous cellular composition and/or the proximity to other cell layers, spectral blending could not be avoided for Hilus/CA4, ventricular, and CA2 regions, for FTIR imaging. As such, these regions were subsequently excluded from the study. (B) Regions of interest for which average XFM elemental areal density was calculated:CC = corpus callosum; SO = stratum oriens; SP = stratum pyramidal; SR = stratum radiatum; SL = stratum lucidum (mossy fibers); IC = internal capsule; SG = stratum granulsom; SM = stratum molecular inner; SML = stratum molecular outer; SUB HCF = subiculum hippocampal formation; CA1 = cornus amonnis sector 1; CA2 = cornus amonnis sector 2; CA3 = cornus amonnis sector 3, which was further subdivided into CA3 ab, and CA3 c; DG = dentate gyrus; (C) Representative FTIR image showing hippocampal lipid distribution, which demonstrates the ability to visually identify hippocampal sub-regions. (D) Representative XFM tri-colour elemental overlay of K, Fe, Zn areal-densities. Scale bar = 500 µm.

FTIR Spectroscopic Imaging Does Not Reveal Evidence of Protein Aggregates, Proteinaceous Deposits, or Amyloid Plaques in the Hippocampus of 4 Month Old Adult SAMP8 Mice

Many studies report an increased incidence of protein aggregates or proteinaceous deposits in the brain during natural ageing, and in Alzheimer's disease, in both humans and animal models.[66-69] In

the case of Alzheimer's disease, the extra-cellular deposits are enriched in the Aβ fragment of APP, *i.e.*, the Aβ-plaque, and intra-cellular deposits are enriched in hyper-phosphorylated tau.[66-68] In the SAMP8 strain, studies have shown a mild age related increase in brain APP expression in SAMP8 mice, and a mild age related increase in Presilin 1 (PS-1), an enzyme responsible for cleavage of the Aβ fragment from APP.[9, 10] However, Aβ -plaques are not detected at the same time-points (4 – 12 months).[10] Micro Aβ-plaques have been confirmed in much older SAMP8 mice (21 months of age).[10] A confounding factor in previous work using antibodies to detect Aβ, has been the report of "Aβ-granules",[70, 71] which do not produce positive staining with Thioflavin S or Congo Red.[70, 71] Subsequent studies have suggested the granules are an artefact of minute trace contamination of the anti-body. Several studies have since positively identified that "Aβ-granules" observed in aged mice are in fact carbohydrate enriched granulated deposits, stained by neo-epitopes, and are not Aβ-plaques, nor do they contain Aβ or APP.[19, 20, 72]

In this investigation, we have used FTIR spectroscopic imaging, a method which is gaining increased use in the field of neuroscience,[39, 43, 48, 51, 52, 55-58, 63, 73-79] as a direct method to test for the presence of aggregated protein. The carbonyl moiety of amide bonds is highly sensitive to hydrogen bonding, which is heavily influenced by protein secondary structure. The relationship between protein secondary structure and carbonyl hydrogen bonding gives rise to characteristic shifts of the amide I band in FTIR spectra, which act as a fingerprint for protein secondary structure. We have previously used FTIR to characterise aggregated protein associated with amyloid plaques in the APP/PS1 model of Alzheimer's disease (Figure 2A,D).[41, 73] As can be seen from comparison of hippocampal tissue from an APP/PS1 mouse relative to SAMP8 or SAMR1 mice (Figure 2A-G), there is no evidence for the presence of protein aggregates in SAMP8 and SAMR1 mice, at the time point studied. These results are in good agreement with the literature and suggest that Aβ-plaque pathology is unlikely to be a major component driving cognitive decline and dementia in the SAMP8 model.[10]

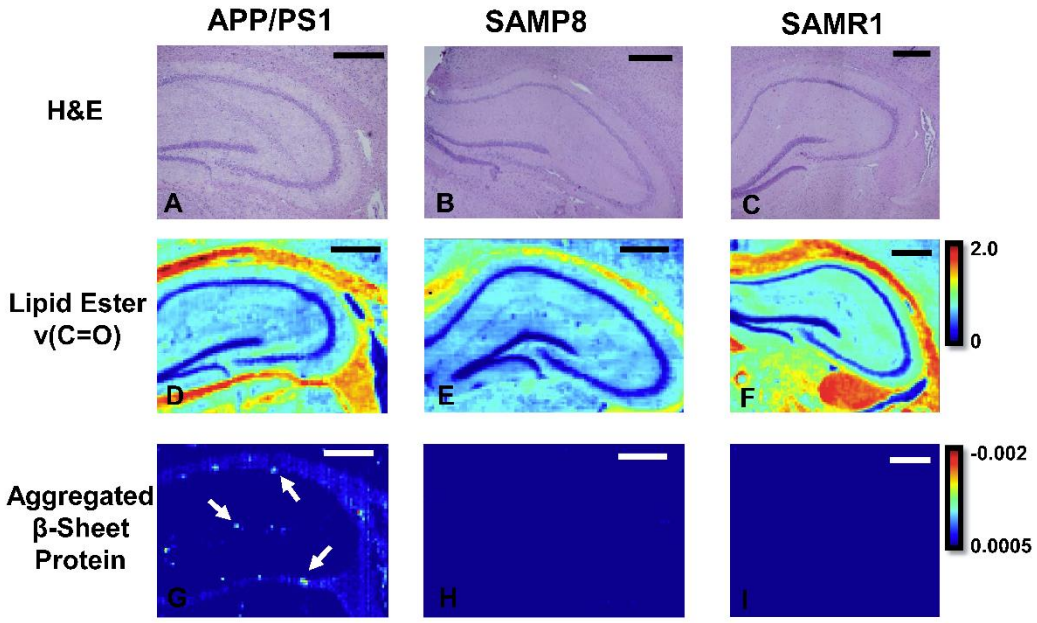

Figure 2: Evaluation of protein aggregation in APP/PS1 transgenic mice (A, D, G) and SAMP8 (B, E, G) and SAMR1 (C, F, I) mice, which highlights that the extensive aggregated protein deposits in APP/PS1 mice are absent in both SAMP8 and SAMR1 mice. (A-C) Routine H&E histology of hippocampus. (D-E) FTIR imaging of hippocampal lipid ester distribution, to reveal hippocampal anatomy. (G-I) Distribution of protein aggregates (second-derivative intensity at 1625 cm-1). White arrows highlight multiple aggregates are present in the hippocampus of APP/PS1 mice. Scale bar = 500 μm.

FTIR Spectroscopic Imaging Reveals Disturbed Energy Metabolism is Most Pronounced in Corpus Callosum White Matter in 4 Month Old Adult SAMP8 Mice Relative to SAMR1 Mice

It is well established that disturbed energy metabolism and increased lactate production is a feature of the ageing brain, in humans and rodents.[24, 80] Past work by others, in rodent models, has demonstrated increased brain lactate during ageing, from bulk analysis of brain homogenates using biochemical assay, chromatography, nuclear magnetic resonance (NMR) spectroscopy, or magnetic resonance imaging (MRI).[24, 25, 80] However, a limitation of biochemical assay is that the spatial distribution of lactate is lost during tissue homogenisation, and MRI provides a spatial resolution on the order of hundreds of microns, at best. Therefore, there is still ambiguity surrounding the exact brain locations and structures responsible of increased lactate production during ageing.

FTIR spectroscopy has limited chemical specificity when compared to biochemical assays or NMR, nor does it offer *in vivo* imaging, however, a spectroscopic marker sensitive to lactate in brain tissue exists in the mid-infrared spectroscopic range, the lactate ν(C-O) at 1127 cm^{-1}.[31, 39, 46] In this study, FTIR spectroscopy has been used to study the relative lactate content of the hippocampus and surrounding corpus callosum at a meso-scale spatial resolution of 25 µm (Figure 3 and Figure 4). The results highlight that in both SAMP8 and SAMR1 mice, lactate levels are highest in the pyramidal cell layers within the hippocampus. However, no statistically significant difference in lactate content was observed within hippocampal sub-regions between SAMP8 and SAMR1 mice. In contrast, a statistically significant increase in relative lactate content was observed within corpus callosum white matter in the brains of 4 month old SAMP8 mice relative to SAMR1 mice.

The localisation of increased lactate content within the corpus callosum white matter of SAMP8 mice, but not the hippocampus proper, is intriguing. The cellular origin of the lactate has not been investigated in this study, however, it is well established oligodendrocytes have high metabolic needs for myelin synthesis, and disturbance of their metabolism or lipid homeostasis could manifest in lactate accumulation.[81-84] Given the high abundance of oligodendrocytes within white matter, we tentatively speculate that these findings suggest disturbed oligodendrocyte metabolism in the SAMP8 strain. Our observation of disturbed lipid homeostasis within the corpus callosum of SAMP8 mice (discussed below) provides further evidence for disturbed glia homeostasis. However, further studies will be required to address this finding in more detail.

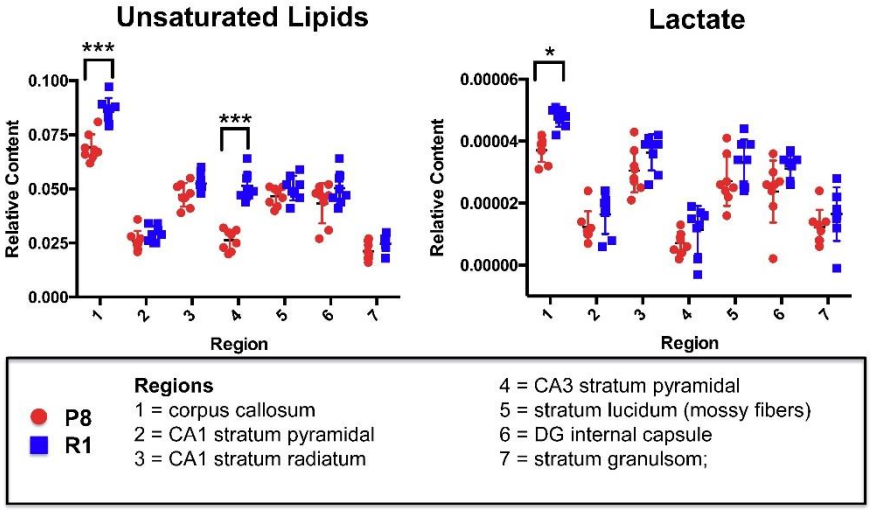

Figure 3: FTIR Spectrosocpic imaging analyses of biochemical markers: unsaturated lipid olefinic groups (A); and lactate (B). The results for additional markers (lipid methylene groups, lipid esters) are presented in Supporting Information.Post-hoc t-tests were used to identify statistically significant differences between the SAMP8 and SAMR1 strains, n = 8 animals in each group. *$p < 0.05$, **$p < 0.01$ ***$p < 0.0001$, Bonferroni corrected for 20 multiple comparisons. Data are presented as mean ± standard deviation, *p*-value for lactate comparison = 0.0113 (corpus callosum). The anatomical location of the sub-regions are shown in Figure 1B.

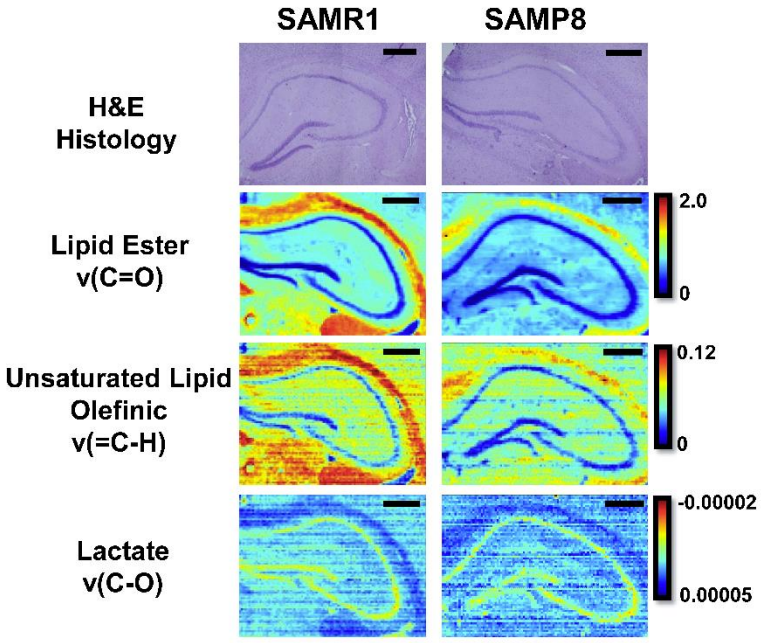

Figure 4: Representative FTIR spectroscopic imaging of markers of lipid homeostasis: total lipid esters; lipid methylene groups; lipid unsaturation (olefinic groups); and metabolic markers (lactate), in SAMP8 and SAMR1 mice. A uniform intensity scale is used for each marker, allowing semi-quantitative comparison between SAMP8 and SAMR1 images. The images visually show the decreased lipid levels in corpus callosum white matter in SAMP8 mice relative to SAMR1 mice, supporting the statistically significant differences reported in Figure 3. Although the greatest relative lactate content was observed in hippocampal neuronal layers for both SAMP8 and SAMR1 mice (yellow pixels), these images reflect the higher relative lactate content within the corpus callosum of SAMP8 mice (light blue pixels) compared to SAMR1 mice (dark blue pixels). Scale bar = 500 µm.

FTIR Spectroscopic Imaging Reveals Evidence of Disturbed Lipid Homeostasis in SAMP8 Mice in the Corpus Callosum White Matter and CA3 Pyramidal Neurons

Recent in vivo MRI T2 weighted imaging of rodent and human brains during ageing has identified early changes in specific brain white matter regions (white matter hyper-intensities) that coincide with the earliest signs of dementia related cognitive impairment.[85-89] Such findings, confined to brain white matter, may suggest a role of altered lipid homeostasis in the initial stages of dementia development. In addition, altered lipid homeostasis within the corpus callosum has previously been reported by FTIR imaging in murine models of Alzheimer's disease.[42] However, few studies have been able to localise age-related lipid alterations to cerebral white matter, *in situ*, or co-localise lipid alterations with metabolic alterations, such as increased lactate production. Extending from the results discussed above for relative white matter lactate content, we used FTIR spectroscopic imaging to determine if lipid alterations were also present in cerebral white matter, or other hippocampal regions.

For the first time, we have identified a reduction in markers of lipid unsaturation (decreased levels of lipid olefinic groups), which colocalise with increased lactate in cerebral white matter, in 4 month old SAMP8 mice relative to age matched SAMR1 mice (Figure 3, Figure 4). In addition to the observation of decrease in lipid unsaturation within the corpus callosum white matter, subtle but statistically significant decrease in lipid unsaturation was also observed in the pyramidal neurons of the CA3 subsector of the hippocampus. Within the corpus callosum white matter, oligodendrocytes are the cell responsible for axon myelination and have an enormous metabolic capacity that is required for

ongoing myelin production and maintenance. There is substantive supporting evidence within the literature that oligodendrocytes under stress may utilise anaerobic metabolism to meet the energy demands associated myelin synthesis and repair.[81-84] As such, increased lactate levels and an altered lipid profile in corpus callosum white matter may indicate oligodendrocyte pathology in the SAMP8 strain. Therefore, future studies are now required to monitor the time course changes in lactate and lipid homeostasis in the corpus callosum over a lifelong time course in the SAMP8 and SAMR1 strains.

XFM Reveals Altered Hippocampal Metal Homeostasis in SAMP8 Mice, However, Increased Levels of Redox Active Metals are Not Present at 4 months of Age Relative to SAMR1 Mice

In addition to FTIR spectroscopic imaging, XFM analyses were used to reveal elemental alterations that may occur concomitant with the observed biochemical changes. Numerous studies by others have demonstrated substantive evidence that redox active metals accumulate during ageing, promoting oxidative stress and macromolecular oxidation. Interestingly, despite the pronounced biochemical alterations observed in the corpus callosum white matter, we detected no statistically significant differences in elemental content in this brain region (Figure 5).

Surprisingly, analysis of elemental content across all other hippocampal sub-regions also failed to demonstrate evidence for elevated metal levels in SAMP8 mice relative to SAMR1 mice. In fact, a statistically significant decrease in Zn was observed in the CA3 mossy fibers (Figure 5 and Figure 6). Although elevated metal content was not observed, this study does not preclude the involvement of metals in accelerated ageing in the SAMP8 model. Firstly, this study has only investigated one time point, early adult mice (4 months old). It is entirely possible that although elevated metal content is not present at 4 months of age, metal levels will increase in SAMP8 mice at later time points, driving cognitive decline reported in this animal model. Alternatively, although the total metal content is not increased at this time point, specific pools of labile, redox active metals may have increased, which would not be detected by measurement of total metal content. Recently, micro X-ray absorption spectroscopy has been demonstrated capable of imaging metal redox states in biological systems, which we intend to incorporate in future SAMP8 mice studies, to investigate redox state alterations in the absence of alterations in total metal content.

The decreased Zn levels observed in the CA3 mossy fibre sub-region are intriguing, as Zn bioavailability holds important roles in brain function/malfunction. It is well established that Zn has an important neuro-modulatory role within the hippocampus, and reduced Zn levels in the mossy fibres correlate with impaired memory.[90-92] In this investigation, we demonstrate for the first time a statistically significant decrease in total Zn content of the CA3 mossy fibre region in SAMP8 mice (Figure 3 and Figure 5), which may account in part for the cognitive deficits that are known to occur in these mice. Interestingly, although Zn levels have not previously been evaluated in SAMP8 mice, fluorescence Zn probes have provided evidence for decreased labile Zn pools in SAMP10 mice, another SAMP strain that experiences accelerated ageing and cognitive decline.[90] Therefore, although only one time point has been studied so far, in addition to testing the hypothesis that metal accumulation may drive oxidative stress and cognitive decline during ageing, the SAMP model may serve to test an alternate hypothesis in future studies, specifically, that metal bioavailability is essential for memory function and metal deficiencies during ageing may also contribute to memory loss. At this stage it is not known if the decreased lipid unsaturation levels within the CA3 pyramidal neurons is related to the decreased Zn levels in the mossy fibres, however, future time-course studies will help elucidate the timeline of development for these changes during animal aging.

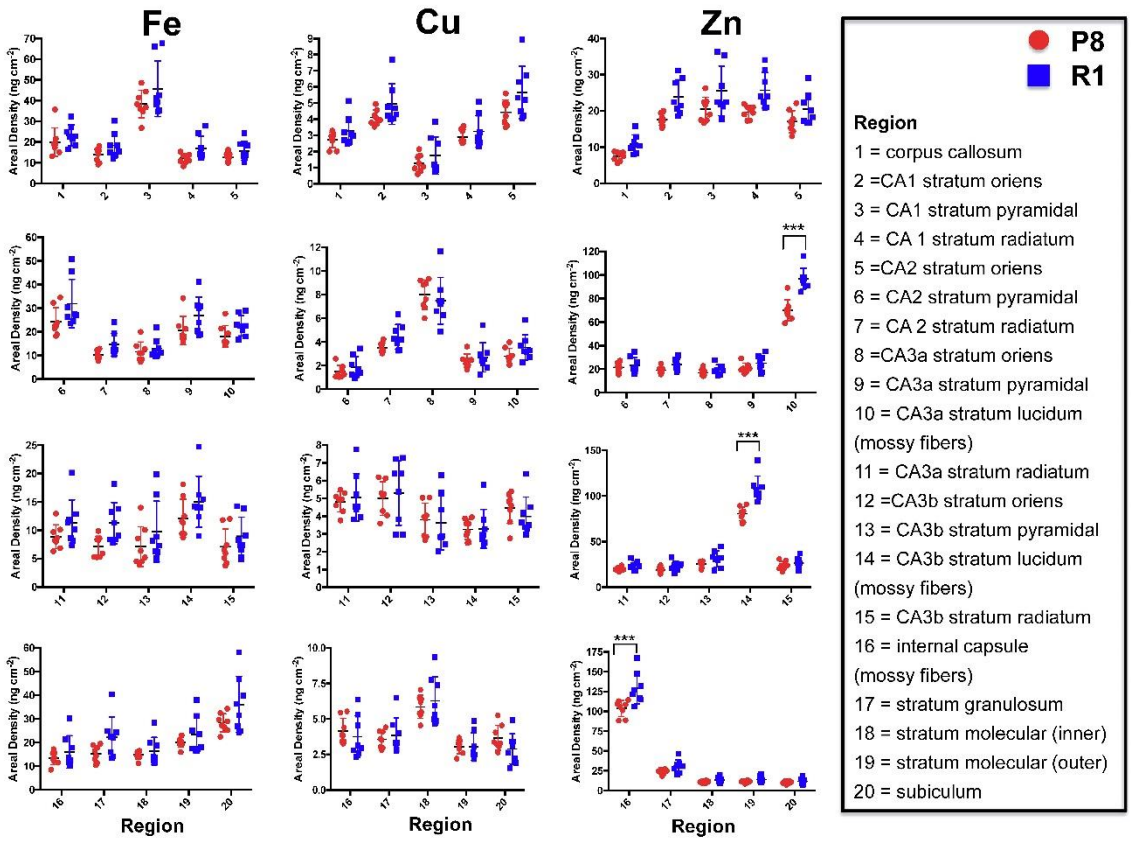

Figure 5: XFM analysis of hippocampal elemental areal densities for Zn (A, B), Cu (C, D) and Fe (E, F). The results for additional elements (P, S, Cl, K, and Ca) are presented in Supporting Information. Post-hoc t-tests were used to identify statistically significant differences between the SAMP8 and SAMR1 strains, n = 8 animals in each group. *$p < 0.05$, **$p < 0.01$ ***$p < 0.0001$, Bonferroni corrected for 20 multiple comparisons. Data are presented as mean ± standard deviation. The anatomical location of the sub-regions are shown in Figure 1B.

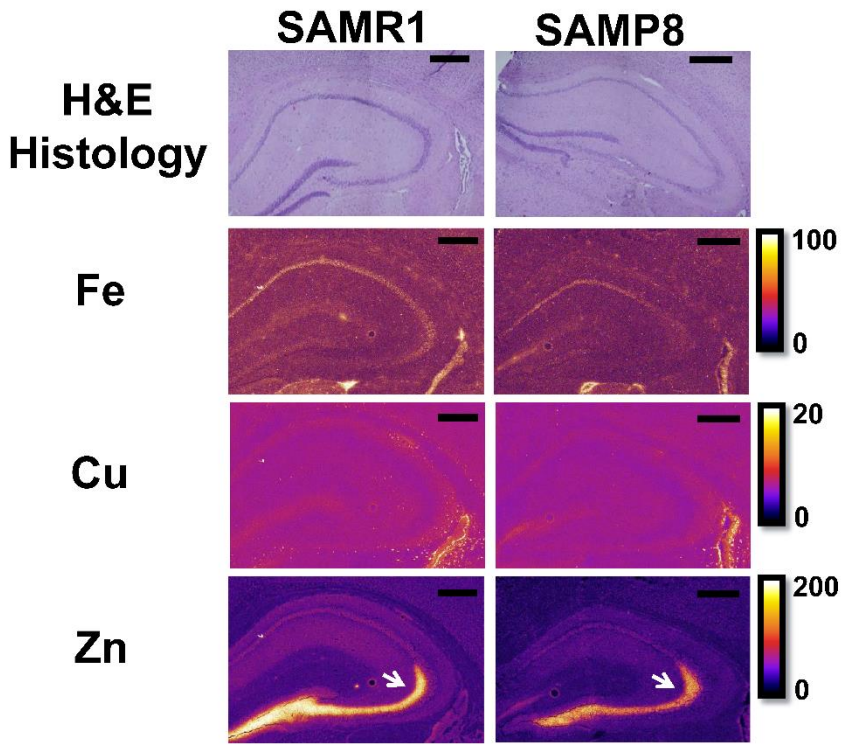

Figure 6: Representative XFM areal density maps (ng cm^{-2}) of hippocampal Fe, Cu and Zn in SAMP8 and SAMR1 mice. A uniform intensity scale is used for each element, allowing quantitative comparison between SAMP8 and SAMR1 images. The images visually show the alterations in metal homeostasis in SAMP8 mice relative to SAMR1 mice, supporting the average values presented in Figure 5. A statistically significant difference in Zn content was observed in the mossy fiber layer of the CA3 sub-sector of SAMP8 mice relative to SAMR1 mice (white arrows). CA = cornus amonnis. Scale bar = 500 µm.

XFM Reveals Distinct but Scattered Punctate Cu Deposits in SAMR1 Mice, which are Absent in SAMP8 Mice

On average, we detected no statistically significant difference in Cu levels across the entire hippocampus, or within any specific sub-region (Figure 5 and Figure 6). However, qualitatively XFM elemental mapping revealed the presence of numerous discrete punctate Cu hots spots within the hippocampus of SAMR1 mice, but not SAMP8 mice (Figure 7). Both mice strains displayed high Cu content in the sub-ventricular zone of the lateral ventricles, which has been reported by several authors in mice and rats.[37, 62, 93, 94] However, in addition to Cu enriched cells along the ependymal wall and sub-ventricular zone, there appeared to be numerous Cu enriched cells radiating from the sub-ventricular zone and into the hippocampus in the SAMR1 mice (Figure 7). At this stage the cellular identity of the Cu hotspots is not known, but will be investigated in future studies, in addition to monitoring alterations to Cu content within these cells, and the total number of Cu-enriched-cells, during aging.

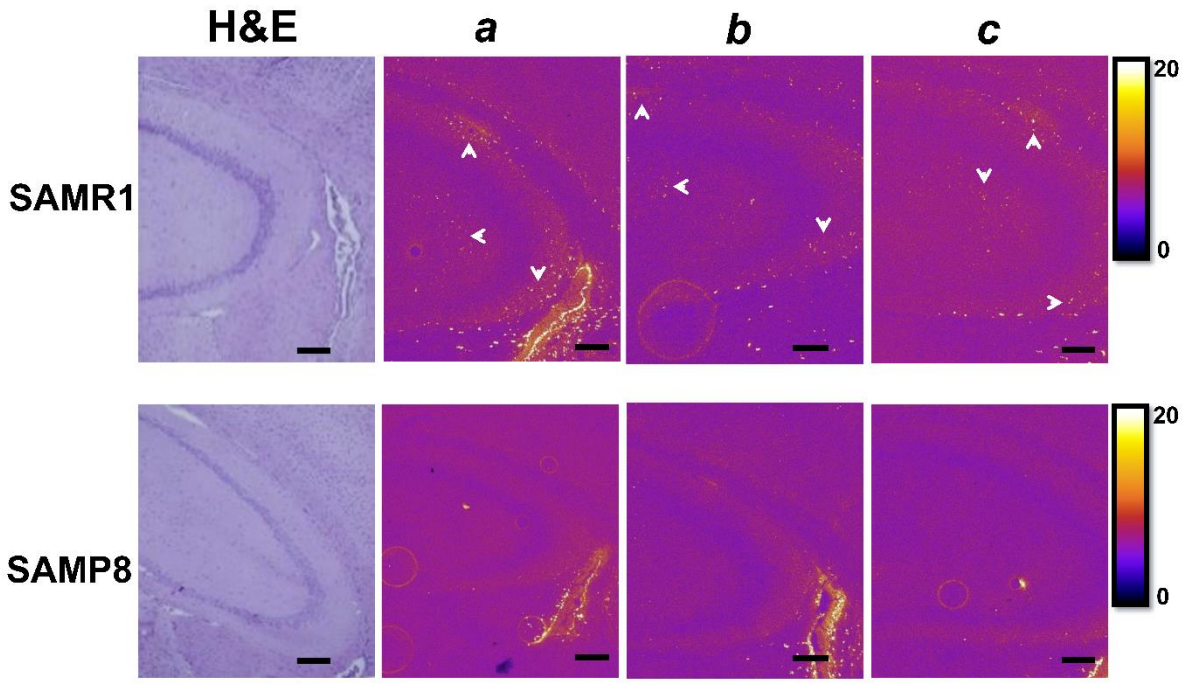

Figure 7: Qualitative analysis of XFM elemental areal density maps (ng cm^{-2}) reveals the presence of numerous punctate Cu "hotspots", most likely cells enriched in Cu (white arrows), within the hippocampus of SAMR1 mice compared to SAMP8 mice. Both SAMP8 and SAMR1 mice display high Cu levels around lateral ventricles. Representative images are shown for 3 separate animals (a, b, c), from SAMP8 and SAMR1 groups. Scale bars = 100 µm.

CONCLUSIONS

Although we can only speculate as to the origin of the observed biochemical and elemental alterations between SAMP8 and SAMR1 mice, this study has made an important first step in identifying a series of biochemical and elemental differences between adult SAMP8 and SAMR1 mice. The identified biochemical differences will now be monitored in a full time course study of SAMP8 and SAMR1 mice, from post-natal, through adolescence, adulthood and into senescence. In our current study, FTIR imaging has provided the first direct observation of concomitant altered lipid homeostasis and increased lactate levels in corpus callosum white matter. This finding may indicate altered oligodendrocyte function, and provides a putative physiological mechanism for the white matter hyper-intensities observed in T2 weighted MRI, which are becoming an important early clinical diagnostic marker of dementia. Surprisingly, we did not detect elevated metals concomitant with the biochemical changes in the corpus callosum or other hippocampal regions. However, the decreased levels of Zn observed within the hippocampus may contribute in part, to the memory deficits others have observed in the SAMP8 strain. Lastly, our study further emphasises the important role that direct spectroscopic imaging techniques such as FTIR and XFM can hold in the field of neuroscience, as they provide direct localisation of important biochemical and elemental markers at the meso- and micro-scales, which is often not possible with more traditional techniques.

METHODS

Animal models

SAMP8 (n = 8) and SAMR1 (n = 8) mice were housed in standard cages in a temperature controlled (21 °C) colony room on a 12/12 h light/dark cycle with standard rodent maintenance chow and water available *ad libitum*. All experimental procedures were conducted in accordance with Curtin University Animal Ethics Guidelines.

The transgenic amyloid precursor protein/presenilin-1 (APP/PS1) mouse tissue for image comparison in Figure 2, was surplus from a larger time course study, and our previous publication.[41]

Tissue Collection and Sample Preparation

To best preserve the *in vivo* biochemical and elemental content and to avoid introduction of chemical artefacts that can result during sample preparation, mice were anaesthetized with pentobarbitone (45 mg/kg), humanely sacrificed, and the brain tissue rapidly removed from the skull, dissected along a sagittal mid-line, and the right hemisphere plunge-flash-frozen in liquid nitrogen cooled isopentane.[31, 33, 34] Serial 10-µm-thick coronal brain sections were cut with a cryo-microtome at -18 ˚C and melted onto: a silicon nitride substrate (Melbourne Centre for Nanofabrication) for XFM analyses; 1mm thick CaF_2 substrate (Crystran) for FTIR analyses, and regular glass microscope slides for routine histology. The silicon nitride substrate consisted of a 10 × 10 mm^2 200 µm thick silicon frame, and a 5 × 5 mm^2 1000 nm thick silicon nitride membrane.

Synchrotron X-ray Fluorescence Microscopy

Elemental mapping of tissue sections was performed at the X-ray Fluorescence Microscopy beamline at the Australian Synchrotron.[47] These methods have been published prior (as cited in the following text), but are described in brief below, with citations available for original report describing the more detailed method. A monochromatic incident beam of energy 15.8 keV was focused to a ~1 µm (1-sigma) spot with a Kirkpatrick–Baez mirror pair and X-ray emissions from the sample were collected in event-mode using the low-latency, 384-channel Maia detector.[48] Data were collected with the sample oriented normal to the incident beam and with the detector positioned in backscatter geometry. The sample was raster scanned through the beam with an effective dwell time of 0.1 ms per effective step (image pixel) size of 1 µm. Images were collected with a 1 µm pixel size, and post data collection images were processed with a 3 point moving average to increase signal to noise and enhance image contrast. Elemental foils (Micromatter, Canada), were scanned in the same geometry, as references for elemental quantification. Elemental maps of areal density were reconstructed from the full emission spectra with GeoPIXE v6.6j (CSIRO, Australia), using a linear transformation matrix for spectral deconvolution. Quantification was performed with calibration against elemental foils of known composition, taking into account composition and density of the silicon nitride substrate, the approximate composition of the sample, and air path between the sample and detector elements. The composition of the tissue sample was approximated as dried organic material ($C_{22}H_{10}N_2O_4$), with a density of 1.42 g cm^{-3}, as in our previous studies.[37, 41] The sample was approximated to have shrunk normal to its plane of sectioning, by a factor of ~3 during air-drying, to a final thickness of 3.5 µm. Quantitatively analysed data were extracted as TIFF files of per-pixel elemental areal density in ng cm^{-2}, which were then imported into ImageJ v1.48, as described previously.[37, 41]

FTIR Spectroscopic Data Collection

FTIR spectroscopic images of tissue sections were collected with a Nicolet iN 10MX FTIR microscope, with an 8x2 pixel liquid nitrogen cooled linear array detector and 25 µm pixel size. Spectra were collected at 4 cm^{-1} spectral resolution with 16 co-added scans. A background image was collected under the same conditions and scanning parameters, using a blank CaF2 substrate.

FTIR Spectroscopic Data Analysis

FTIR spectra were analysed with Cytospec v2.00.03 and OPUS v7.0. For analysis of relative aggregated protein content and relative lactate content, second-derivative spectra were calculated from vector normalized raw spectra (vector normalized to the amide I band, 1700 – 1600 cm^{-1}), using a 9 smoothing point Savitzky-Golay function. FTIR false colour images of aggregated protein and lactate distribution were generated from second-derivative intensity at 1625 cm^{-1} and 1127 cm^{-1}, respectively. Analysis of lipid homeostasis was performed from images of lipid ester, lipid methylene and lipid olefinics, which were generated from the area under the curve of the ester carbonyl band (1755 – 1715 cm^{-1}) lipid methylene groups $\nu_s(CH_2)$ (2865 – 2840 cm^{-1}) and olefinic ν(C-H) (3025 – 3000 cm^{-1}), using a linear background subtraction across the same spectral range, in non-normalised and non-derivatised spectra. For statistical analysis, regions of interest were calculated from FTIR images, for the anatomical regions described above, and the average area under the peak or second-derivative intensity calculated as per original image generation.

Histology and Fluorescence Microscopy

Serial tissue sections were post-fixed in 10% buffered formalin (Sigma) and stained, following a routine haematoxylin and eosin (H&E) protocol. Microscopy images of H&E stained tissue were collected at 4x magnification using a Olympus Bx51 microscope with Olympus dp70 camera and cellSans Standard software.

Statistical Analysis

The dependent variables of interest were elemental content (P, S, Cl, K, Ca, Fe, Cu, Zn) and biochemical content (lipid esters, lipid methylene groups, olefinic groups, and lactate). Data were analysed using a 2-Way repeated measures ANOVA, with strain (SAMP8 vs SAMR1) treated as a between-subjects factor and anatomical location (see figure caption for Figure 1) as a within-subjects factor. Statistically significant interactions were followed by post-hoc t-tests corrected for 20 multiple corrections using the Bonferroni method. Alpha was set at 0.05. Figures present the individual data points for each animal for each condition, along with the group mean ± standard deviation (σ). All statistical analysis was performed using GraphPad Prism v7.04. Post-hoc testing for differences in elemental or biochemical composition between anatomical regions within the same animal strain was not performed in this study.

SUPPORTING INFORMATION

In addition to the findings reported in this manuscript (Fe, Cu, Zn, lactate, and unsaturated lipids), XFM and FTIR analyses revealed elemental distribution of P, S, Cl, K, Ca and the biochemical distributions of lipid esters and lipid methylene groups. Data for these variables are presented in Supporting Information in addition to a copy of the 2-Way ANOVA report.

ABBREVIATIONS

XFM = X-ray fluorescence microscopy

FTIR = Fourier transform infrared spectroscopy

SAMP8 = senescence accelerated murine prone, strain 8

SAMR1 = senescence accelerated murine resistant, strain 1

AUTHOR INFORMATION

Corresponding Author

*Dr Mark J. Hackett E-mail: mark.j.hackett@curtin.edu.au Tel.: +61 8 9266 3102

AUTHOR CONTRIBUTIONS

The manuscript was written and edited through contributions of all authors. All authors have given approval to the final version of the manuscript.

Nicholas Fimognari (PhD Student, co – first – author) Formulated scientific ideas with Ashley Hollings, and performed XFM data collection and analysis. Contributed to writing first manuscript draft

Ashley Hollings (PhD Student, co – first – author) Formulated scientific ideas with Nicholas Fimognari and performed FTIR data collection and analysis. Contributed to writing first manuscript draft

Virginie Lam (Post doc) Generated tissue from animal model, assisted Nick Fimognari with sample preparation, performed tissue histochemistry

Rebecca J. Tidy (Honours student) Prepared tissue sections, and assisted in FTIR and Raman data collection and analysis

Cameron Kewish (Beamline Scientist) Assisted in XFM data collection and data analysis at the Australian Synchrotron.

Matthew Albrecht (Co-Investigator) Assisted with design of revised statistical analysis.

Ryu Takechi (Research Fellow, Co-Investigator), Supervisor of NF. Assisted in generating tissue samples from SAMP8 and SAMR1 animal model and assisted in statistical analysis with MA.

John C.L. Mamo (Co-Investigator), Supervisor of NF. Assisted with conceptual design of FTIR and XFM experiments, and edited manuscript.

Mark J. Hackett (Corresponding Author), Supervisor of RJT, AH, NF. Responsible for overviewing data collection, data analysis, editing student manuscript drafts and revisions. Lead role is experimental design.

ACKNOWLEDGEMENTS

JM and RT are supported by the Australian National Health and Medical Research Council, Department of Health, Australian Government (APP1064567). MJH is supported by the Dementia Australia Research Foundation, Mamutil New Investigator Project Grant (11646). We gratefully acknowledge travel funding provided by ANSTO, funded by the Australian Government. Components of this research were undertaken at the X-ray fluorescence Microscopy (XFM) beamline at the Australian Synchrotron, ANSTO, Victoria, Australia. We gratefully thank Peter Chapman, Daryl Howard, Martin de Jonge and David Paterson for assistance in training with aspects of FTIR, and XFM data collection and data analysis.

References

1. (2015) The Global Impact of Dementia: An analysis of prevalence, incidence, cost and trends. World Alzheimer Report, Alzheimer's Disease International

2. Butterfield, D. A., and Poon, H. F. (2005) The senescence-accelerated prone mouse (SAMP8): A model of age-related cognitive decline with relevance to alterations of the gene expression and protein abnormalities in Alzheimer's disease, Exp. Gerontol. 40, 774-783.

3. Flood, J. F., and E. Morley, J. (1997) Learning and memory in the SAMP8 mouse, Neurosci. Biobehav. Rev. 22, 1-20.

4. Pallas, M., Camins, A., Smith, M. A., Perry, G., Lee, H.-g., and Casadesus, G. (2008) From aging to Alzheimer's disease: unveiling" the switch" with the senescence-accelerated mouse model (SAMP8), J. Alzheimer's Dis. 15, 615-624.

5. Takeda, T., Hosokawa, M., and Higuchi, K. (1997) Senescence-accelerated mouse (SAM): a novel murine model of senescence, Exp. Gerontol. 32, 105-109.

6. Takeda, T., Hosokawa, M., Higuchi, K., Hosono, M., Akiguchi, I., and Katoh, H. (1994) A novel murine model of aging, Senescence-Accelerated Mouse (SAM), Arch. Gerontol. Geriatr. 19, 185-192.

7. del Valle, J., Duran-Vilaregut, J., Manich, G., Camins, A., Pallàs, M., Vilaplana, J., and Pelegrí, C. (2009) Time-course of blood–brain barrier disruption in senescence-accelerated mouse prone 8 (SAMP8) mice, Int. J. Dev. Neurosci. 27, 47-52.

8. Ueno, M., Akiguchi, I., Hosokawa, M., Shinnou, M., Sakamoto, H., Takemura, M., and Higuchi, K. (1997) Age-related changes in the brain transfer of blood-borne horseradish peroxidase in the hippocampus of senescence-accelerated mouse, Acta Neuropathol. 93, 233-240.

9. Kumar, V. B., Franko, M., Banks, W. A., Kasinadhuni, P., Farr, S. A., Vyas, K., Choudhuri, V., and Morley, J. E. (2009) Increase in Presenilin 1 (PS1) levels in senescence-accelerated mice (SAMP8) may indirectly impair memory by affecting amyloid precursor protein (APP) processing, J. Exp. Biol. 212, 494-498.

10. Morley, J. E., Kumar, V. B., Bernardo, A. E., Farr, S. A., Uezu, K., Tumosa, N., and Flood, J. F. (2000) β-Amyloid precursor polypeptide in SAMP8 mice affects learning and memory, Peptides 21, 1761-1767.

11. Harigaya, Y., Younkin, S., Yang, F., and Cole, G. (1996) Correlative Memory Deficits, AP3 Elevation, and Amyloid Plaques in Transgenic Mice, Science 274, 4.

12. Games, D., Adams, D., Alessandrini, R., Barbour, R., Borthelette, P., Blackwell, C., Carr, T., Clemens, J., Donaldson, T., Gillespie, F., Guido, T., Hagopian, S., Johnson-Wood, K., Khan, K., Lee, M., Leibowitz, P., Lieberburg, I., Little, S., Masliah, E., McConlogue, L., Montoya-Zavala, M., Mucke, L., Paganini, L., Penniman, E., Power, M., Schenk, D., Seubert, P., Snyder, B., Soriano, F., Tan, H., Vitale, J., Wadsworth, S., Wolozin, B., and Zhao, J. (1995) Alzheimer-type neuropathology in transgenic mice overexpressing V717F [beta]-amyloid precursor protein, Nature 373, 523-527.

13. Oddo, S., Caccamo, A., Shepherd, J. D., Murphy, M. P., Golde, T. E., Kayed, R., Metherate, R., Mattson, M. P., Akbari, Y., and LaFerla, F. M. (2003) Triple-transgenic model of Alzheimer's disease with plaques and tangles: intracellular Aβ and synaptic dysfunction, Neuron 39, 409-421.

14. Sturchler-Pierrat, C., Abramowski, D., Duke, M., Wiederhold, K.-H., Mistl, C., Rothacher, S., Ledermann, B., Bürki, K., Frey, P., and Paganetti, P. A. (1997) Two amyloid precursor protein

transgenic mouse models with Alzheimer disease-like pathology, Proc. Natl. Acad. Sci. U. S. A 94, 13287-13292.

15. Holcomb, L., Gordon, M. N., McGowan, E., Yu, X., Benkovic, S., Jantzen, P., Wright, K., Saad, I., Mueller, R., and Morgan, D. (1998) Accelerated Alzheimer-type phenotype in transgenic mice carrying both mutant amyloid precursor protein and presenilin 1 transgenes, Nat. Med. 4, 97-100.

16. Hsiao, K., Chapman, P., Nilsen, S., Eckman, C., Harigaya, Y., Younkin, S., Yang, F., and Cole, G. (1996) Correlative Memory Deficits, Aβ Elevation, and Amyloid Plaques in Transgenic Mice, Science 274, 99-103.

17. Hardy, J., and Selkoe, D. J. (2002) The amyloid hypothesis of Alzheimer's disease: progress and problems on the road to therapeutics, Science 297, 353-356.

18. Wisniewski, T., Ghiso, J., and Frangione, B. (1997) Biology of Aβ Amyloid in Alzheimer's Disease, Neurobiol. Dis. 4, 313-328.

19. Manich, G., Augé, E., Cabezón, I., Pallàs, M., Vilaplana, J., and Pelegrí, C. (2015) Neo-epitopes emerging in the degenerative hippocampal granules of aged mice can be recognized by natural IgM auto-antibodies, Immun. Ageing : I & A 12, 23.

20. Manich, G., del Valle, J., Cabezón, I., Camins, A., Pallàs, M., Pelegrí, C., and Vilaplana, J. (2014) Presence of a neo-epitope and absence of amyloid beta and tau protein in degenerative hippocampal granules of aged mice, Age 36, 151-165.

21. Shibata, M., Yamada, S., Kumar, S. R., Calero, M., Bading, J., Frangione, B., Holtzman, D. M., Miller, C. A., Strickland, D. K., Ghiso, J., and Zlokovic, B. V. (2000) Clearance of Alzheimer's amyloid-β(1-40) peptide from brain by LDL receptor–related protein-1 at the blood-brain barrier, J. Clin. Invest. 106, 1489-1499.

22. Pelegrí, C., Canudas, A. M., del Valle, J., Casadesus, G., Smith, M. A., Camins, A., Pallàs, M., and Vilaplana, J. (2007) Increased permeability of blood–brain barrier on the hippocampus of a murine model of senescence, Mech. Ageing Dev. 128, 522-528.

23. Ueno, M., Sakamoto, H., Kanenishi, K., Onodera, M., Akiguchi, I., and Hosokawa, M. (2001) Ultrastructural and permeability features of microvessels in the hippocampus, cerebellum and pons of senescence-accelerated mice (SAM), Neurobiol. Aging 22, 469-478.

24. Ross, J. M., Öberg, J., Brené, S., Coppotelli, G., Terzioglu, M., Pernold, K., Goiny, M., Sitnikov, R., Kehr, J., Trifunovic, A., Larsson, N.-G., Hoffer, B. J., and Olson, L. (2010) High brain lactate is a hallmark of aging and caused by a shift in the lactate dehydrogenase A/B ratio, Proc. Natl. Acad. Sci. U. S. A. 107, 20087-20092.

25. Jiang, N., Yan, X., Zhou, W., Zhang, Q., Chen, H., Zhang, Y., and Zhang, X. (2008) NMR-Based Metabonomic Investigations into the Metabolic Profile of the Senescence-Accelerated Mouse, J. Proteome Res. 7, 3678-3686.

26. Adlard, P. A., and Bush, A. I. (2006) Metals and Alzheimer's disease, J. Alzheimer's Dis. 10, 145-163.

27. Maynard, C. J., Bush, A. I., Masters, C. L., Cappai, R., and Li, Q.-X. (2005) Metals and amyloid-β in Alzheimer's disease, Int. J. Exp. Pathol. 86, 147-159.

28. Braidy, N., Poljak, A., Marjo, C., Rutlidge, H., Rich, A., Jugder, B.-E., Jayasena, T., Inestrosa, N. C., and Sachdev, P. S. (2017) Identification of Cerebral Metal Ion Imbalance in the Brain of Aging Octodon degus, Front. Aging Neurosci. 9, 66.

29. Focht, S. J., Snyder, B. S., Beard, J. L., Van Gelder, W., Williams, L. R., and Connor, J. R. (1997) Regional distribution of iron, transferrin, ferritin, and oxidatively-modified proteins in young and aged Fischer 344 rat brains, Neuroscience 79, 255-261.

30. Zecca, L., Youdim, M. B. H., Riederer, P., Connor, J. R., and Crichton, R. R. (2004) Iron, brain ageing and neurodegenerative disorders, Nat. Rev. Neurosci. 5, 863-873.

31. Hackett, M. J., Britz, C. J., Nichol, H., Paterson, P. G., Pickering, I. J., and George, G. N. (2015) In situ Bio-Spectroscopic Investigation of Rapid Ischemic and Post-mortem Induced Biochemical Alterations in the Rat Brain, ACS Chem. Neurosci. 6, 226-238.

32. Hackett, M. J., Lee, J., El-Assaad, F., McQuillan, J. A., Carter, E. A., Grau, G. E., Hunt, N. H., and Lay, P. A. (2012) FTIR Imaging of Brain Tissue Reveals Crystalline Creatine Deposits Are an ex Vivo Marker of Localized Ischemia during Murine Cerebral Malaria: General Implications for Disease Neurochemistry, ACS Chem. Neurosci. 3, 1017-1024.

33. Hackett, M. J., McQuillan, J. A., El-Assaad, F., Aitken, J. B., Levina, A., Cohen, D. D., Siegele, R., Carter, E. A., Grau, G. E., Hunt, N. H., and Lay, P. A. (2011) Chemical alterations to murine brain tissue induced by formalin fixation: implications for biospectroscopic imaging and mapping studies of disease pathogenesis, Analyst 136, 2941-2952.

34. Hackett, M. J., Smith, S. E., Paterson, P. G., Nichol, H., Pickering, I. J., and George, G. N. (2012) X-ray Absorption Spectroscopy at the Sulfur K-Edge: A New Tool to Investigate the Biochemical Mechanisms of Neurodegeneration, ACS Chem. Neurosci. 3, 178-185.

35. Chwiej, J., Szczerbowska-Boruchowska, M., Lankosz, M., Wojcik, S., Falkenberg, G., Stegowski, Z., and Setkowicz, Z. (2005) Preparation of tissue samples for X-ray fluorescence microscopy, Spectrochim. Acta B 60, 1531-1537.

36. Matsuyama, S., Shimura, M., Fujii, M., Maeshima, K., Yumoto, H., Mimura, H., Sano, Y., Yabashi, M., Nishino, Y., and Tamasaku, K. (2010) Elemental mapping of frozen-hydrated cells with cryo-scanning X-ray fluorescence microscopy, X-Ray Spectrom. 39, 260-266.

37. Lins, B. R., Pushie, J. M., Jones, M., Howard, D. L., Howland, J. G., and Hackett, M. J. (2016) Mapping Alterations to the Endogenous Elemental Distribution within the Lateral Ventricles and Choroid Plexus in Brain Disorders Using X-Ray Fluorescence Imaging, PLoS One 11, e0158152.

38. Williamson, M. R., Dietrich, K., Hackett, M. J., Caine, S., Nadeau, C. A., Aziz, J. R., Nichol, H., Paterson, P. G., and Colbourne, F. (2016) Rehabilitation Augments Hematoma Clearance and Attenuates Oxidative Injury and Ion Dyshomeostasis After Brain Hemorrhage, Stroke 48, 195-203.

39. Hackett, M. J., Aitken, J. B., El-Assaad, F., McQuillan, J. A., Carter, E. A., Ball, H. J., Tobin, M. J., Paterson, D., de Jonge, M. D., Siegele, R., Cohen, D. D., Vogt, S., Grau, G. E., Hunt, N. H., and Lay, P. A. (2015) Mechanisms of murine cerebral malaria: Multimodal imaging of altered cerebral metabolism and protein oxidation at hemorrhage sites, Science Advances 1, e1500911.

40. Silasi, G., Klahr, A. C., Hackett, M. J., Auriat, A. M., Nichol, H., and Colbourne, F. (2012) Prolonged therapeutic hypothermia does not adversely impact neuroplasticity after global ischemia in rats, J. Cereb. Blood Flow Metab. 32, 1525-1534.

41. Summers, K. L., Fimognari, N., Hollings, A., Kiernan, M., Lam, V., Tidy, R. J., Paterson, D., Tobin, M. J., Takechi, R., George, G. N., Pickering, I. J., Mamo, J. C., Harris, H. H., and Hackett, M. J. (2017) A Multimodal Spectroscopic Imaging Method To Characterize the Metal and Macromolecular Content of Proteinaceous Aggregates (“Amyloid Plaques”), Biochemistry 56, 4107-4116.

42. Leskovjan, A. C., Kretlow, A., and Miller, L. M. (2010) Fourier Transform Infrared Imaging Showing Reduced Unsaturated Lipid Content in the Hippocampus of a Mouse Model of Alzheimer's Disease, Anal. Chem. 82, 2711-2716.

43. Liao, C. R., Rak, M., Lund, J., Unger, M., Platt, E., Albensi, B. C., Hirschmugl, C. J., and Gough, K. M. (2013) Synchrotron FTIR reveals lipid around and within amyloid plaques in transgenic mice and Alzheimer's disease brain, Analyst 138, 3991-3997.

44. Benseny-Cases, N., Klementieva, O., Cotte, M., Ferrer, I., and Cladera, J. (2014) Microspectroscopy (μFTIR) Reveals Co-localization of Lipid Oxidation and Amyloid Plaques in Human Alzheimer Disease Brains, Anal. Chem. 86, 12047-12054.

45. Heraud, P., Caine, S., Campanale, N., Karnezis, T., McNaughton, D., Wood, B. R., Tobin, M. J., and Bernard, C. C. A. (2009) Early Dectection of the Chemical Changes Occurring During the Induction and Prevention of Autoimmune-mediated Demyelination Detected by FT-IR Imaging, NeuroImage 49, 1180-1189.

46. Hackett, M. J., Sylvain, N. J., Hou, H., Caine, S., Alaverdashvili, M., Pushie, M. J., and Kelly, M. E. (2016) Concurrent Glycogen and Lactate Imaging with FTIR Spectroscopy to Spatially Localize Metabolic Parameters of the Glial Response following Brain Ischemia, Anal. Chem.

47. Chwiej, J., Dulinska, J., Janeczko, K., Appel, K., and Setkowicz, Z. (2012) Variations in elemental compositions of rat hippocampal formation between acute and latent phases of pilocarpine-induced epilepsy: an X-ray fluorescence microscopy study, JBIC Journal of Biological Inorganic Chemistry 17, 731-739.

48. Chwiej, J., Dulinska, J., Janeczko, K., Dumas, P., Eichert, D., Dudala, J., and Setkowicz, Z. (2010) Synchrotron FTIR micro-spectroscopy study of the rat hippocampal formation after pilocarpine-evoked seizures, J. Chem. Neuroanat. 40, 140-147.

49. Chwiej, J., Kutorasinska, J., Janeczko, K., Gzielo-Jurek, K., Uram, L., Appel, K., Simon, R., and Setkowicz, Z. (2012) Progress of elemental anomalies of hippocampal formation in the pilocarpine model of temporal lobe epilepsy: an X-ray fluorescence microscopy study, Anal. Bioanal. Chem. 404, 3071-3080.

50. Chwiej, J., Winiarski, W., Ciarach, M., Janeczko, K., Lankosz, M., Rickers, K., and Setkowicz, Z. (2008) The role of trace elements in the pathogenesis and progress of pilocarpine-induced epileptic seizures, JBIC Journal of Biological Inorganic Chemistry 13, 1267-1274.

51. Caine, S., Hackett, M. J., Hou, H., Kumar, S., Maley, J., Ivanishvili, Z., Suen, B., Szmigielski, A., Jiang, Z., Sylvain, N. J., Nichol, H., and Kelly, M. E. (2016) A novel multi-modal platform to image molecular and elemental alterations in ischemic stroke, Neurobiol. Dis. 91, 132-142.

52. Hackett, M. J., DeSouza, M., Caine, S., Bewer, B., Nichol, H., Paterson, P. G., and Colbourne, F. (2015) A New Method To Image Heme-Fe, Total Fe, and Aggregated Protein Levels after Intracerebral Hemorrhage, ACS Chem. Neurosci. 6, 761-770.

53. Bourassa, M. W., Leskovjan, A. C., Tappero, R. V., Farquhar, E. R., Colton, C. A., Van Nostrand, W. E., and Miller, L. M. (2013) Elevated copper in the amyloid plaques and iron in the cortex are observed in mouse models of Alzheimer’s disease that exhibit neurodegeneration, Biomedical spectroscopy and imaging 2, 129-139.

54. Leskovjan, A. C., Lanzirotti, A., and Miller, L. M. (2009) Amyloid plaques in PSAPP mice bind less metal than plaques in human Alzheimer's disease, NeuroImage 47, 1215-1220.

55. Miller, L. M., Wang, Q., Telivala, T. P., Smith, R. J., Lanzirotti, A., and Miklossy, J. (2006) Synchrotron-based infrared and X-ray imaging shows focalized accumulation of Cu and Zn co-localized with beta-amyloid deposits in Alzheimer's disease, J. Struct. Biol. 155, 30-37.

56. Kastyak-Ibrahim, M. Z., Nasse, M. J., Rak, M., Hirschmugl, C., Del Bigio, M. R., Albensi, B. C., and Gough, K. M. (2012) Biochemical label-free tissue imaging with subcellular-resolution synchrotron FTIR with focal plane array detector, NeuroImage 60, 376-383.

57. Kuzyk, A., Kastyak, M., Agrawal, V., Gallant, M., Sivakumar, G., Rak, M., Del Bigio, M. R., Westaway, D., Julian, R., and Gough, K. M. (2010) Association among amyloid plaque, lipid, and creatine in hippocampus of TgCRND8 mouse model for Alzheimer disease, J. Biol. Chem. 285, 31202-31207.

58. Surowka, A. D., Pilling, M., Henderson, A., Boutin, H., Christie, L., Szczerbowska-Boruchowska, M., and Gardner, P. (2017) FTIR imaging of the molecular burden around A[small beta] deposits in an early-stage 3-Tg-APP-PSP1-TAU mouse model of Alzheimer's disease, Analyst 142, 156-168.

59. James, S. A., Churches, Q. I., de Jonge, M. D., Birchall, I. E., Streltsov, V., McColl, G., Adlard, P. A., and Hare, D. J. (2017) Iron, Copper, and Zinc Concentration in Aβ Plaques in the APP/PS1 Mouse Model of Alzheimer's Disease Correlates with Metal Levels in the Surrounding Neuropil, ACS Chem. Neurosci. 8, 629-637.

60. Szczerbowska-Boruchowska, M., Dumas, P., Kastyak, M. Z., Chwiej, J., Lankosz, M., Adamek, D., and Krygowska-Wajs, A. (2007) Biomolecular investigation of human substantia nigra in Parkinson's disease by synchrotron radiation Fourier transform infrared microspectroscopy, Arch. Biochem. Biophys. 459, 241-248.

61. Popescu, B. F., Frischer, J. M., Webb, S. M., Tham, M., Adiele, R. C., Robinson, C. A., Fitz-Gibbon, P. D., Weigand, S. D., Metz, I., Nehzati, S., George, G. N., Pickering, I. J., Brück, W., Hametner, S., Lassmann, H., Parisi, J. E., Yong, G., and Lucchinetti, C. F. (2017) Pathogenic implications of distinct patterns of iron and zinc in chronic MS lesions, Acta Neuropathol. 134, 45-64.

62. Pushie, M. J., Pickering, I. J., Martin, G. R., Tsutsui, S., Jirik, F. R., and George, G. N. (2011) Prion protein expression level alters regional copper, iron and zinc content in the mouse brain, Metallomics 3, 206-214.

63. Kneipp, J., Miller, L. M., Joncic, M., Kittel, M., Lasch, P., Beekes, M., and Naumann, D. (2003) In situ identification of protein structural changes in prion-infected tissue, Biochim. Biophys. Acta 1639, 152-158.

64. Wang, Q., Kretlow, A., Beekes, M., Naumann, D., and Miller, L. (2005) In situ characterization of prion protein structure and metal accumulation in scrapie-infected cells by synchrotron infrared and X-ray imaging, Vib. Spectrosc 38, 61-69.

65. Miyamoto, M. (1997) Characteristics of age-related behavioral changes in senescence-accelerated mouse SAMP8 and SAMP10, Exp. Gerontol. 32, 139-148.

66. Grune, T., Jung, T., Merker, K., and Davies, K. J. A. (2004) Decreased proteolysis caused by protein aggregates, inclusion bodies, plaques, lipofuscin, ceroid, and 'aggresomes' during oxidative stress, aging, and disease, Int. J. Biochem. Cell Biol. 36, 2519-2530.

67. Keller, J. N., Dimayuga, E., Chen, Q., Thorpe, J., Gee, J., and Ding, Q. (2004) Autophagy, proteasomes, lipofuscin, and oxidative stress in the aging brain, Int. J. Biochem. Cell Biol. 36, 2376-2391.

68. Butterfield, D. A., and Kanski, J. (2001) Brain protein oxidation in age-related neurodegenerative disorders that are associated with aggregated proteins, Mech. Ageing Dev. 122, 945-962.

69. Jucker, M., Walker, L., Schwarb, P., Hengemihle, J., Kuo, H., Snow, A., Bamert, F., and Ingram, D. (1994) Age-related deposition of glia-associated fibrillar material in brains of C57BL/6 mice, Neuroscience 60, 875-889.

70. Fukunari, A., Kato, A., Sakai, Y., Yoshimoto, T., Ishiura, S., Suzuki, K., and Nakajima, T. (1994) Colocalization of prolyl endopeptidase and amyloid β-peptide in brains of senescence-accelerated mouse, Neurosci. Lett. 176, 201-204.

71. Takemura, M., Nakamura, S., Akiguchi, I., Ueno, M., Oka, N., Ishikawa, S., Shimada, A., Kimura, J., and Takeda, T. (1993) Beta/A4 proteinlike immunoreactive granular structures in the brain of senescence-accelerated mouse, Am. J. Pathol. 142, 1887-1897.

72. Jucker, M., Walker, L. C., Schwarb, P., Hengemihle, J., Kuo, H., Snow, A. D., Bamert, F., and Ingram, D. K. (1994) Age-related deposition of glia-associated fibrillar material in brains of c57BL/6 mice, Neuroscience 60, 875-889.

73. Tidy, R. J., Lam, V., Fimognari, N., Mamo, J. C., and Hackett, M. J. (2017) FTIR studies of the similarities between pathology induced protein aggregation in vivo and chemically induced protein aggregation ex vivo, Vib. Spectrosc. 91, 68-76.

74. Summers, K. L., Fimognari, N., Hollings, A., Kiernan, M., Lam, V., Tidy, R. J., Paterson, D., Tobin, M. J., Takechi, R., and George, G. N. (2017) A Multimodal Spectroscopic Imaging Method To Characterize the Metal and Macromolecular Content of Proteinaceous Aggregates ("Amyloid Plaques"), Biochemistry 56, 4107-4116.

75. Hackett, M. J., Smith, S. E., Caine, S., Nichol, H., George, G. N., Pickering, I. J., and Paterson, P. G. (2015) Novel bio-spectroscopic imaging reveals disturbed protein homeostasis and thiol redox with protein aggregation prior to hippocampal CA1 pyramidal neuron death induced by global brain ischemia in the rat, Free Radical Biol. Med. 89, 806-818.

76. Gough, K. M., Tzadu, L., Kastyak, M. Z., Kuzyk, A. C., and Julian, R. L. (2010) Theoretical and experimental considerations for interpretation of amide I bands in tissue, Vib. Spectrosc. 53, 71-76.

77. Gelfand, P., Smith, R. J., Stavitski, E., Borchelt, D. R., and Miller, L. M. (2015) Characterization of Protein Structural Changes in Living Cells Using Time-Lapsed FTIR Imaging, Anal. Chem. 87, 6025-6031.

78. Kretlow, A., Wang, Q., Kneipp, J., Lasch, P., Beekes, M., Miller, L., and Naumann, D. (2006) FTIR-microspectroscopy of prion-infected nervous tissue, Biochim. Biophys. Acta 1758, 948-959.

79. Miller, L. M., Bourassa, M. W., and Smith, R. J. (2013) FTIR spectroscopic imaging of protein aggregation in living cells, Biochim. Biophys. Acta 1828, 2339-2346.

80. Beal, M. F. (1995) Aging, energy, and oxidative stress in neurodegenerative diseases, Ann. Neurol. 38, 357-366.

81. Rao, V. T. S., Khan, D., Cui, Q.-L., Fuh, S.-C., Hossain, S., Almazan, G., Multhaup, G., Healy, L. M., Kennedy, T. E., and Antel, J. P. (2017) Distinct age and differentiation-state dependent metabolic profiles of oligodendrocytes under optimal and stress conditions, PLoS One 12, e0182372.

82. Sánchez-Abarca, L. I., Tabernero, A., and Medina, J. M. (2001) Oligodendrocytes use lactate as a source of energy and as a precursor of lipids, Glia 36, 321-329.

83. Ichihara, Y., Doi, T., Ryu, Y., Nagao, M., Sawada, Y., and Ogata, T. (2017) Oligodendrocyte Progenitor Cells Directly Utilize Lactate for Promoting Cell Cycling and Differentiation, J. Cell. Physiol. 232, 986-995.

84. Rinholm, J. E., and Bergersen, L. H. (2014) White matter lactate – Does it matter?, Neuroscience 276, 109-116.

85. Debette, S., and Markus, H. S. (2010) The clinical importance of white matter hyperintensities on brain magnetic resonance imaging: systematic review and meta-analysis, BMJ 341, c3666.

86. Duan, J.-H., Wang, H.-Q., Xu, J., Lin, X., Chen, S.-Q., Kang, Z., and Yao, Z.-B. (2006) White matter damage of patients with Alzheimer's disease correlated with the decreased cognitive function, Surg. Radiol. Anat. 28, 150-156.

87. Magnaldi, S., Ukman, M., Vasciaveo, A., Longo, R., and Pozzi-Mucelli, R. S. (1993) Contrast between white and grey matter: MRI appearance with ageing, Eur. Radiol. 3, 513-519.

88. Naggara, O., Oppenheim, C., Rieu, D., Raoux, N., Rodrigo, S., Dalla Barba, G., and Meder, J.-F. (2006) Diffusion tensor imaging in early Alzheimer's disease, Psychiatry Research: Neuroimaging 146, 243-249.

89. Salat, D. H., Tuch, D. S., Hevelone, N. D., Fischl, B., Corkin, S., Rosas, H. D., and Dale, A. M. (2005) Age-Related Changes in Prefrontal White Matter Measured by Diffusion Tensor Imaging, Ann. N. Y. Acad. Sci. 1064, 37-49.

90. Saito, T., Takahashi, K., Nakagawa, N., Hosokawa, T., Kurasaki, M., Yamanoshita, O., Yamamoto, Y., Sasaki, H., Nagashima, K., and Fujita, H. (2000) Deficiencies of Hippocampal Zn and ZnT3 Accelerate Brain Aging of Rat, Biochem. Biophys. Res. Commun. 279, 505-511.

91. Adlard, P. A., Parncutt, J. M., Finkelstein, D. I., and Bush, A. I. (2010) Cognitive loss in zinc transporter-3 knock-out mice: a phenocopy for the synaptic and memory deficits of Alzheimer's disease?, J. Neurosci. 30, 1631-1636.

92. Frederickson, C. J., Koh, J.-Y., and Bush, A. I. (2005) The neurobiology of zinc in health and disease, Nat. Rev. Neurosci. 6, 449-462.

93. Pushkar, Y., Robison, G., Sullivan, B., Fu, S. X., Kohne, M., Jiang, W., Rohr, S., Lai, B., Marcus, M. A., and Zakharova, T. (2013) Aging results in copper accumulations in glial fibrillary acidic protein-positive cells in the subventricular zone, Aging cell 12, 823-832.

94. Robison, G., Zakharova, T., Fu, S., Jiang, W., Fulper, R., Barrea, R., Marcus, M. A., Zheng, W., and Pushkar, Y. (2012) X-ray fluorescence imaging: a new tool for studying manganese neurotoxicity, PLoS One 7, e48899.